Performance of Immuno – Positron Emission Tomography with Zirconium-89-Labeled Chimeric Monoclonal Antibody U36 in the Detection of Lymph Node Metastases in Head and Neck Cancer Patients

Pontus K.E. Börjesson,[1] Yvonne W.S. Jauw,[1] Ronald Boellaard,[2] Remco de Bree,[1] Emile F.I. Comans,[2] Jan C. Roos,[2] Jonas A. Castelijns,[3] Maria J.W.D. Vosjan,[1] J. Alain Kummer,[4] C. René Leemans,[1] Adriaan A. Lammertsma,[2] and Guus A.M.S. van Dongen[1,2]

Abstract

Purpose: Immuno – positron emission tomography (PET), the combination of PET with monoclonal antibodies (mAb), is an attractive option to improve tumor detection and to guide mAb-based therapy. The long-lived positron emitter zirconium-89 (^{89}Zr) has ideal physical characteristics for immuno-PET with intact mAbs but has never been used in a clinical setting. In the present feasibility study, we aimed to evaluate the diagnostic imaging performance of immuno-PET with ^{89}Zr-labeled-chimeric mAb (cmAb) U36 in patients with squamous cell carcinoma of the head and neck (HNSCC), who were at high risk of having neck lymph node metastases.

Experimental Design: Twenty HNSCC patients, scheduled to undergo neck dissection with or without resection of the primary tumor, received 75 MBq ^{89}Zr coupled to the anti-CD44v6 cmAb U36 (10 mg). All patients were examined by computed tomography (CT) and/or magnetic resonance imaging (MRI) and immuno-PET before surgery. Six patients also underwent PET with ^{18}F-fluoro-2-deoxy-D-glucose. Immuno-PET scans were acquired up to 144 hours after injection. Diagnostic findings were recorded per neck side (left or right) as well as per lymph node level (six levels per side), and compared with histopathologic outcome. For this purpose, the CT/MRI scores were combined and the best of both scores was used for analysis.

Results: Immuno-PET detected all primary tumors (n = 17) as well as lymph node metastases in 18 of 25 positive levels (sensitivity 72%) and in 11 of 15 positive sides (sensitivity 73%). Interpretation of immuno-PET was correct in 112 of 121 operated levels (accuracy 93%) and in 19 of 25 operated sides (accuracy 76%). For CT/MRI, sensitivities of 60% and 73% and accuracies of 90% and 80% were found per level and side, respectively. In the six patients with seven tumor-involved neck levels and sides, immuno-PET and ^{18}F-fluoro-2-deoxy-D-glucose PET gave comparable diagnostic results.

Conclusion: In this study, immuno-PET with ^{89}Zr-cmAb U36 performed at least as good as CT/MRI for detection of HNSCC lymph node metastases.

Radiolabeled monoclonal antibodies (mAb) have shown considerable potential for diagnosis and treatment of cancer (1, 2). In clinical radioimmunoscintigraphy and radioimmunotherapy studies done at our institute, the potential of the CD44v6-specific murine mAb (mmAb) U36 for these purposes has been shown. Radioimmunoscintigraphy with technetium-99m (^{99m}Tc)-labeled mmAb U36 IgG was found to be as reliable as the radiological imaging techniques computed tomography (CT) and magnetic resonance imaging (MRI) for the detection of lymph node metastases in patients with head and neck squamous cell carcinoma (HNSCC), but the detection of tumor deposits smaller than 1 cm seemed to be a problem despite the proven accumulation of the mAb in these tumors (3). Subsequently, chimeric mAb (cmAb) U36 was tested in clinical phase I dose escalation radioimmunotherapy trials (4, 5). Promising antitumor effects were observed with ^{186}Re-cmAb U36 in HNSCC patients with end-stage disease.

Introduction of immuno-PET, the combination of PET with mAbs, is an attractive option to improve tumor detection because it combines the high sensitivity and resolution of a PET camera with the specificity of a mAb (6–8). The latter might be an advantage in comparison with the currently used PET tracers such as fluorine-18-labeled fluoro-2-deoxy-D-glucose

Authors' Affiliations: Departments of [1]Otolaryngology/Head and Neck Surgery, [2]Nuclear Medicine and Positron Emission Tomography Research, [3]Radiology, and [4]Pathology, VU University Medical Center, Amsterdam, the Netherlands

Received 10/10/05; revised 1/9/06; accepted 1/26/06.

Grant support: Dutch Cancer Society grant IKA VU2000-2155.

The costs of publication of this article were defrayed in part by the payment of page charges. This article must therefore be hereby marked *advertisement* in accordance with 18 U.S.C. Section 1734 solely to indicate this fact.

Requests for reprints: Guus A.M.S. van Dongen, Department of Otolaryngology/Head and Neck Surgery, VU University Medical Center, De Boelelaan 1117, 1081 HV Amsterdam, the Netherlands. Phone 31-20-4440953; Fax: 31-20-4443688; E-mail: gams.vandongen@VUmc.nl.

doi:10.1158/1078-0432.CCR-05-2137

(^{18}FDG), which shows increased uptake not only in tumors but also in normal tissues with high metabolic activity. Apart from its diagnostic capabilities, PET also has potential for quantification of molecular interactions, which is particularly attractive when immuno-PET is used as prelude to antibody-based therapy. First, patients can be selected who have the best chance to benefit from mAb treatment (6–8). Next, in an individualized therapeutic approach, immuno-PET enables the confirmation of tumor targeting and the quantification of mAb accumulation in tumor and normal tissues. For this purpose, we started the coupling of positron emitters to mAbs and a preclinical evaluation of these radiolabeled mAbs in immuno-PET.

For being suitable for immuno-PET, a positron emitter has to fulfill several requirements. Its physical half-life has to be compatible with the time needed for a mAb to achieve optimal tumor-to-nontumor ratios. For intact mAbs, presently the most frequently used format for targeting solid tumors, this time is generally 2 to 4 days.

Two positron emitters with a proper half-life for immuno-PET with intact mAbs are zirconium-89 (^{89}Zr, half-life 78.4 hours) and iodine-124 (^{124}I, half-life 100.3 hours). Of these isotopes, ^{89}Zr can be obtained with high yield, high radionuclide purity, and low production costs (9). Moreover, ^{89}Zr has ideal characteristics for optimal image quality and accurate quantification. Stable coupling of ^{89}Zr to mAbs was accomplished using the succinylated chelate desferrioxamine B (desferal; ref. 9). The suitability of such conjugates, ^{89}Zr-labeled cmAb U36 included, for detection of millimeter-sized tumors was shown in HNSCC xenograft-bearing nude mice (10). In addition, the potential of PET for quantification of ^{89}Zr-labeled mAbs was shown in these studies (10).

Based on aforementioned encouraging preclinical results, we hypothesized that PET with ^{89}Zr-labeled mAb U36 might be better suited for detection of lymph node metastases in HNSCC patients than previously tested single-photon emission computerized tomography (SPECT) approaches with mAb U36. To the best of our knowledge, the long-lived positron emitter ^{89}Zr has never been tested in a clinical setting before. In the present study, PET with ^{89}Zr-labeled mAb U36 was evaluated for its safety and preliminary diagnostic accuracy in patients with proven HNSCC and clinically at high risk of having lymph node metastases.

Materials and Methods

Patient study. Twenty patients, who were at high risk of having neck lymph node metastasis from a proven HNSCC and who were planned to undergo neck dissection with or without resection of the primary tumor, participated in this study. Decision about the need for neck dissection, and the type of neck dissection, was based on primary tumor site and tumor stage as found by conventional clinical and diagnostic examinations. Immuno-PET did not influence this decision. Confirmation of CD44v6 expression by biopsy was not required, as >96% of tumors show CD44v6 expression by at least 50% of the cells (11). The primary tumor and the status of neck lymph nodes were classified according to the tumor-node-metastasis system of the International Union Against Cancer (12). Patient and tumor characteristics are given in Table 1. Prior and up to 6 weeks after administration of radiolabeled cmAb U36, routine laboratory analyses were done, including complete blood cell counts, serum electrolytes, urine sediment, liver enzymes, and renal and thyroid functions. Vital signs were recorded before and up to 3 hours after injection.

Patients received cmAb U36 IgG radiolabeled with ^{89}Zr (74.9 ± 0.6 MBq). The first 14 patients simultaneously received 55 MBq

Table 1. Patient and tumor characteristics

Patient	Sex	Age	Primary tumor	cTNM	pTNM
1	F	57	Oral cavity, tongue, right	$T_2N_0M_0$	$T_2N_1M_0$
2	M	57	Unknown primary, base of tongue right side suspected	$T_xN_{2a}M_0$	$T_{is}N_{2b}M_0$
3	F	72	Oropharynx, tonsil, right	$T_2N_{2b}M_0$	$T_2N_{2b}M_0$
4	F	53	Oropharynx, tonsil, right	$T_3N_0M_0$	$T_3N_{2b}M_0$
5	M	63	Oropharynx, tonsil, right	$T_4N_0M_0$	$T_4N_{2b}M_0$
6	F	58	Oral cavity, alveolar process and floor of mouth, left	$T_4N_0M_0$	$T_4N_{2b}M_0$
7	M	54	Oral cavity, tongue/floor of mouth, right	$T_3N_0M_0$	$T_3N_{2b}M_0$
8	M	55	Oropharynx, tonsil, left	$T_4N_{2a}M_0$	$T_4N_{2b}M_0$
9	F	54	Hypopharynx, piriform sinus, left	$T_4N_{2b}M_0$	$T_4N_{2b}M_0$
10	F	65	Oral cavity, base of tongue, right	$T_2N_0M_0$	$T_2N_0M_0$
11	M	53	Larynx, glottic	$T_4N_0M_0$	$T_4N_0M_0$
12	M	59	Larynx, supraglottic	$T_4N_0M_0$	$T_4N_0M_0$
13	F	49	Residual disease after T_2N_0 tonsil carcinoma, left	NA	NA
14	M	58	Oropharynx, base of tongue, right	$T_2N_{2b}M_0$	$T_2N_{2b}M_0$
15	M	48	Oropharynx, tonsil, right	$T_3N_0M_0$	$T_3N_1M_0$
16	F	63	Oropharynx, tonsil, left	$T_3N_{2b}M_0$	$T_3N_{2b/c}M_0$
17	M	53	Oropharynx, tonsil, right	$T_2N_3M_0$	$T_2N_3M_0$
18	M	58	Larynx, supraglottic, recurrence	NA	NA
19	M	71	Oropharynx, soft palate, right	$T_3N_{2c}M_0$	$T_2N_{2c}M_0$
20	M	60	Larynx, supraglottic, recurrence	NA	NA

Abbreviations: TNM, tumor-node-metastasis system; cTNM, clinical classification; pTNM, pathologic classification; NA, not applicable.

^{186}Re-labeled cmAb U36 IgG for comparison of pharmacokinetics and biodistribution. This comparison is beyond the scope of the present article and will be reported elsewhere. The total administered cmAb U36 dosage was 10 mg for all patients. Seventeen of 20 patients had surgery of their primary tumor, whereas all patients had unilateral (n = 16) or bilateral (n = 4) neck dissections done 6 to 8 days after administration of radiolabeled cmAb U36. All patients underwent radical neck dissection (patients 2, 14, and 16) or modified radical neck dissection comprising levels I through V, except for patients 11, 12, and 18. Patients 11 and 18 underwent selective bilateral neck dissection (levels II-IV + VI for patient 11, and II-IV for patient 18), whereas patient 12 underwent selective neck dissection (II-IV) on the left side and modified radical neck dissection (level I-VI) on the right side. The study was reviewed and approved by the Medical Ethics Committee of the VU University Medical Center. All patients gave written informed consent after receiving a thorough explanation of the study.

mAb U36. Selection and production of mAb U36 and its chimeric (mouse/human) IgG1 derivative (cmAb U36) have been described previously (4). mAb U36 binds to the v6 region of CD44 (CD44v6). Homogeneous expression of CD44v6 has been observed in squamous cell carcinoma of the head and neck, lung, skin, esophagus, and cervix, whereas heterogeneous expression was found in adenocarcinomas of the breast, lung, colon, pancreas, and stomach. In normal tissues, expression has been found in epithelial tissues, such as skin, breast, and prostate myoepithelium, and bronchial epithelium (13).

Production of ^{89}Zr-cmAb U36. The production and purification of ^{89}Zr and its coupling to cmAb U36 have been described previously (9). ^{89}Zr was produced by a (p,n) reaction on natural yttrium (^{89}Y). Labeling of cmAb U36 was achieved starting from the chelate desferrioxamine B (Df; desferal, Novartis, Basel, Switzerland). All procedures were done under aseptic conditions in a shielded laminar flow hood. In short, Df was succinylated (*N*-sucDf), temporarily filled with stable iron [Fe(III)], and coupled to the lysine residues of cmAb U36 by means of a tetrafluorophenol-*N*-sucDf ester. After removal of Fe(III) by transchelation to EDTA, the premodified cmAb U36 was purified on a PD10 column. Subsequently, *N*-sucDf-cmAb U36 (5 mg) was labeled with^{89}Zr (185 MBq). Finally, ^{89}Zr-*N*-sucDf-cmAb U36 was purified on a PD10 column [eluent: 0.9% NaCl/gentisic 5 mg/mL (pH 5.0)]. ^{89}Zr-*N*-sucDf-cmAb U36 will be abbreviated to ^{89}Zr-cmAb U36 in the rest of this article. The mean labeling efficiency was 87.4 ± 11.0%. Finally, cold cmAb U36 and for 14 of the 20 patients ^{186}Re-MAG3-cmAb U36 were added and the conjugates were filter sterilized (total amount of cmAb U36 to be administered was 10 mg). These procedures resulted in a sterile final product with endotoxin levels <5 EU/mL. The molar ratio *N*-sucDf to cmAb U36 was always <2. The radiochemical purity was always >94.9% (mean, 96.0 ± 1.2%). After each preparation of ^{89}Zr-cmAb U36, the immunoreactivity was determined by measuring binding to a serial dilution of UM-SCC-11B cells as described previously (10). The immunoreactive fraction of the ^{89}Zr-cmAb U36 preparations ranged from 74.8% to 91.0% (mean, 85.1 ± 4.5%) at the highest cell concentration. In addition, the data were graphically analyzed in a modified Lineweaver-Burk plot and the immunoreactivity was determined by extrapolating to conditions representing infinite antigen excess. By doing so, the immunoreactive fraction ranged from 89.4% to 100% (mean, 98.7 ± 3.1%).

Imaging studies. All patients were examined by palpation, CT and/or MRI, and ^{89}Zr-cmAb U36 PET (immuno-PET), whereas six patients were also examined by FDG-PET. The latter procedure was indicated for the detection of unknown primary tumors and/or for screening of distant metastases.

Preoperative palpation was done in all patients by the same experienced head and neck surgeon. CT, MRI, FDG-PET, and immuno-PET were done in 17, 15, 6, and 20 patients, respectively. In all patients, diagnostic examinations and surgery were done within a 3-week period. CT scans were obtained with a third-generation Siemens Somaton Volume Zoom (Siemens AG, Erlangen, Germany). After contrast administration, axial scans with a slice thickness of 3 mm and increment of 3 mm were obtained. MRI examinations were done on a 1.5 T imaging system (Vision-system, Siemens) using a dedicated neck coil. Axial T2-weighed spin-echo, short-term inversion recovery, and pre– and post–gadolinium-diethylenetriaminepentaacetic acid (Magnevist, Schering AG, Germany) T_1-weighed spin-echo MRI examinations were made. Slice thickness varied, depending on the MRI pulse sequence used, from 4 to 7 mm, with an interslice gap of 10%. Criteria for the optimal assessment of cervical lymph node metastases by CT or MRI, as defined by our institute, were used (14). At CT and MRI, lymph nodes were considered malignant if nodes with necrosis were depicted or if the minimal diameter in the axial plane of the node was ≥11 mm for nodes located in level II (subdigastric) and ≥10 mm for nodes in other levels. In routine diagnostic work-up, patients with enlarged lymph nodes of 4 to 11 mm (n = 14) went for additional diagnosis by ultrasound-guided fine-needle aspiration cytology.

PET scans were done using a dedicated full-ring PET scanner (ECAT EXACT HR+, CTI/Siemens, Knoxville, TN). In case of immuno-PET scanning, whole body scans were made consisting of approximately seven bed positions covering the patient from base of the skull to the pelvis. At each bed position, a 3-minute transmission scan, acquired using three germanium-68 rod sources, and a 7-minute emission scan in three-dimensional mode were acquired. Whole body scans were done starting within 1 hour and at 24, 72, and/or 144 hours after i.v. injection of ^{89}Zr-cmAb U36. All scans were normalized and corrected for randoms, scatter, attenuation, and decay. Reconstructions were done using an attenuation and normalization weighted ordered subset expectation maximization algorithm (ECAT software version 7.2, CTI/Siemens) with two iterations and 16 subsets followed by postsmoothing of the reconstructed image using a 5-mm FWHM Gaussian filter. Because images with attenuation correction showed high noise levels due to the low amount of radioactivity administered to the patients (for radiation exposure reasons), ordered subset expectation maximization reconstructions without attenuation correction were done as well. Reconstructions without attenuation correction provided images with a quality similar to that of the diagnostic FDG scans (next paragraph). Interpretation of the scans was therefore done using these non-attenuation-corrected images and was based on asymmetry and retention of activity, especially on late images.

In case of FDG-PET scanning, all patients fasted overnight before the PET study. Whole body scans were made using approximately seven bed positions from the base of the skull to the pelvis. At each bed position, a 7-minute emission scan in two-dimensional mode was made. Scanning started ~ 60 minutes after i.v. injection of 370 MBq ^{18}FDG (Cyclotron BV, Amsterdam, the Netherlands). All scans were corrected as described above for the ^{89}Zr scans; however, no attenuation correction was done. The PET images were evaluated visually using standard ECAT (CTI/Siemens) software: foci with increased uptake versus background were considered abnormal, taking physiologic biodistribution of FDG into account.

CT and MRI were scored by one experienced radiologist (J.A. Castelijns), FDG-PET by one experienced nuclear physician (E.F.I. Comans), whereas immuno-PET examinations were scored by consensus of two experienced nuclear physicians (E.F.I. Comans and J.C. Roos). CT/MRI and nuclear imaging examinations were done in an independent and blinded way, without knowledge of the pathologic outcome. Observers were not informed about the sites of tumor involvement. All patients had neck dissections done 6 to 8 days after the administration of the radioimmunoconjugate. After fixation, all palpable and visible lymph nodes were dissected from the surgical specimen and cut into 2- to 4-mm-thick slices for microscopic examinations. The different slices of one lymph node were examined by a pathologist and the percentage tumor involvement was estimated. The outcome of the histopathologic examination of the neck dissection specimen was used as the gold standard.

For topographical examination, the findings were recorded per side as well as per lymph node level according to the classification of the American Academy of Otorhinolaryngology and Head and Neck Surgery (15). Patients underwent either CT or MRI or both. For

evaluation of overall anatomic imaging results, the data on CT and MRI were combined, and if patients had undergone both diagnostic modalities only the best performing modality was used for analysis.

Human anti-cmAb U36 and anti-N-sucDf-cmAb U36 responses. To evaluate the immunogenicity of cmAb U36 and ^{89}Zr-*N*-sucDf-cmAb U36, a human-anti-cmAb U36 (anti-isotypic) and a human anti-^{89}Zr-*N*-sucDf-cmAb U36 assay were done. Human antibody response was tested in patient sera before administration of ^{89}Zr-*N*-sucDf-cmAb U36 and at 1 and 6 weeks after administration. The concentrations of human anti-cmAb U36 and anti-^{89}Zr-*N*-sucDf-cmAb U36 antibodies were measured essentially as described previously (4). In short, microtiter plates (Costar Europe, Ltd., Badhoevedorp, the Netherlands) were coated with cmAb U36 IgG or with ^{89}Zr-*N*-sucDf-cmAb U36 (after decay), 2 μg/well, in PBS (pH 7.2), and incubated overnight at room temperature. After blocking with assay buffer [PBS with 1% FCS (BioWhittaker, Verviers, Belgium) and 0.02% Tween 20 (Sigma, Zwijndrecht, the Netherlands)] and extensive washing with wash buffer (PBS with 0.05% Tween 20), 100 μL standard dilutions of rabbit anti-human IgG (DAKO, Glostrup, Denmark) and diluted patient serum (1:10 in assay buffer) were pipetted into the wells and incubated for 1 hour at room temperature. Human antichimeric antibody–positive sera from previous clinical trials with cmAb U36 served as reference samples. The rabbit anti-human IgG was used to construct a calibration curve. After extensive washing with wash buffer and PBS, 100 μL biotinylated cmAb U36 or biotinylated ^{89}Zr-*N*-sucDf-cmAb U36 were added (±1 μg/well), and the plate was incubated for 1 hour at room temperature. All subsequent steps, including incubation with horseradish peroxidase–conjugated streptavidin (CLB, Amsterdam, the Netherlands) and tetramethylbenzidine substrate, as well as absorption measurement at 450 nm, were exactly the same as previously described (4). Also, criteria for considering a sample positive were the same (4).

Statistics. In this feasibility study, descriptive statistics were used with assessment of sensitivity, specificity, and accuracy for ^{89}Zr-immuno-PET as well as for the routine diagnostic modalities palpation, CT/MRI, and FDG-PET. This was considered most appropriate because (*a*) in routine diagnostic work-up, CT/MRI might have additional diagnostic value by identification of patients with enlarged lymph nodes (4-11 mm) eligible for ultrasound-guided fine-needle aspiration cytology, (*b*) clinical ^{89}Zr-immuno-PET was used for the first time ever, and therefore it was not known beforehand whether all variables were optimal for tumor detection, e.g., injected ^{89}Zr dose and image acquisition, reconstruction, and evaluation. In addition, procedures for ^{89}Zr quantification are under development and were not available for the present evaluation.

Results

Neither adverse reactions nor significant changes in blood and urine values were observed, which could be related to the injection of the antibody. Patients 9 and 10 developed a human antichimeric antibody response, and elevated titers were found at 1 and 6 weeks postinjection, whether or not cmAb U36 IgG or ^{89}Zr-*N*-sucDf-cmAb U36 was used in the ELISA. These data indicate that the response was directed to the protein part of the conjugate and not to the *N*-succinyldesferrioxamine B chelate attached to the cmAb. None of the samples showed exclusive positivity in the ^{89}Zr-*N*-sucDf-cmAb U36 ELISA, indicating that immunogenicity of the chelate is low.

Whole body images obtained directly after administration of ^{89}Zr-cmAb U36 showed mainly blood-pool activity with delineation of nose, heart, lungs, liver, spleen, and kidneys. Uptake of radioactivity in these organs decreased over time, whereas increased uptake was seen only at tumor sites. No selective accumulation at nontumor sites was observed. Representative whole body scans are shown in Fig. 1.

In the 20 patients studied, all 17 tumors at the primary site were visualized by immuno-PET, including one unknown primary tumor (patient 2). From the 20 patients, lymph nodes present in 25 neck dissections in 121 levels were examined histopathologically for tumor involvement. HNSCC metastases were found in 25 levels in 15 sides. There was no evidence for presence of distant metastases. Representative immuno-PET images of patients with primary tumor and lymph node involvement (patients 16 and 19) are shown in Figs. 2 and 3. Preoperative findings obtained with immuno-PET, palpation, CT/MRI, and for a subgroup of patients with FDG-PET were compared with the histopathologic findings. Sensitivity, specificity, and accuracy of the different diagnostic modalities for detection of lymph node metastases per level and per side in the whole group of patients are shown in Tables 2 and 3. Respective sensitivities of

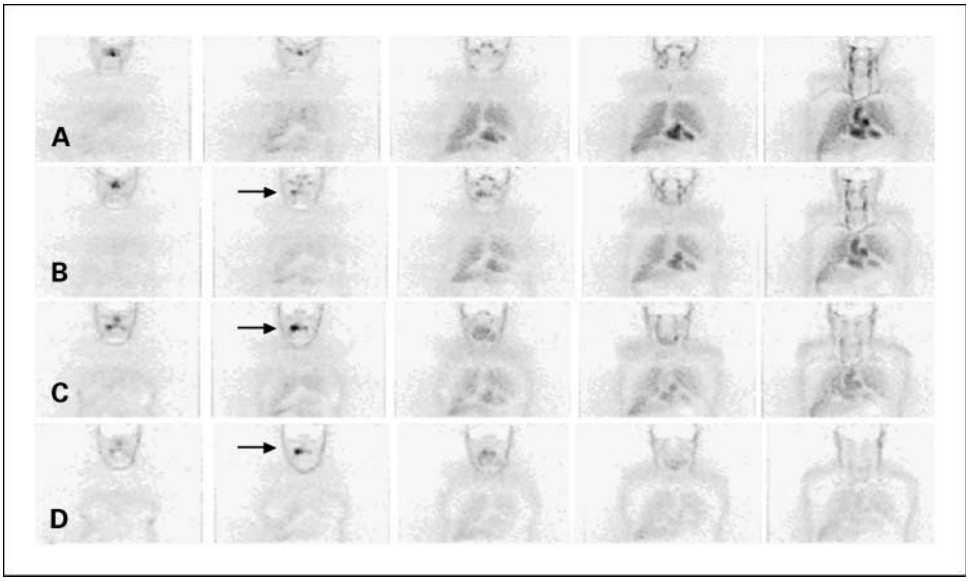

Fig. 1. Immuno-PET images with ^{89}Zr-cmAb U36 of head and neck cancer patient 5, with a tumor of the right tonsil and a lymph node metastasis at the right side of the neck. Images were obtained within 1 hour (*A*), at 24 hours (*B*), at 72 hours (*C*), and at 144 hours (*D*) postinjection. Slices from anterior (*left*) to posterior (*right*). Early images show mainly blood-pool activity with visualization of nose, heart, lungs, and liver. At later images, the primary tumor is clearly visualized (*arrow*). The lymph node metastasis was missed by immuno-PET.

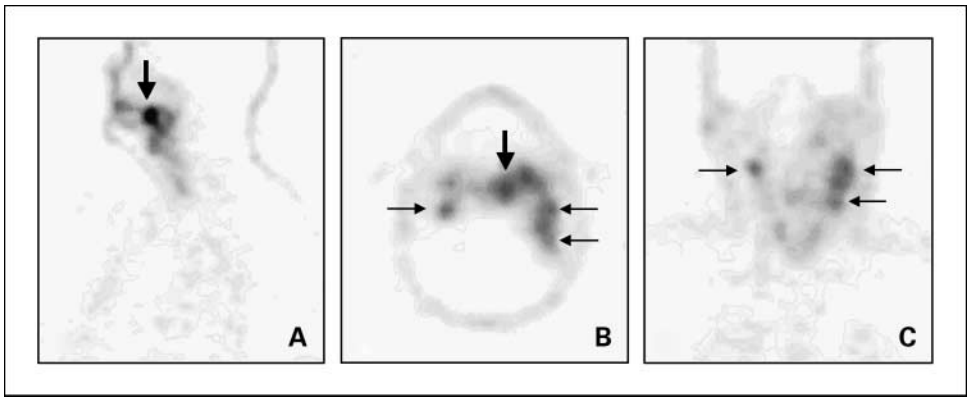

Fig. 2. Immuno-PET images with ^{89}Zr-cmAb U36 of head and neck cancer patient 16, with a tumor in the left tonsil (*large arrow*) and lymph node metastases (*small arrows*) at the left (level II and III) and right (level II) side of the neck. Images were obtained 72 hours postinjection. *A,* sagittal image; *B,* axial image, and *C,* coronal image.

immuno-PET, palpation, and CT/MRI were 72%, 44%, and 60% when evaluated per neck level, and 73%, 53%, and 73% when evaluated per neck side. Accuracy of immuno-PET, palpation, and CT/MRI for the whole group of patients was per level 93%, 88%, and 90%, and per side 76%, 72%, and 80%, respectively.

Six patients also underwent FDG-PET. For these patients, the sensitivity of immuno-PET and FDG-PET for detection of tumor-involved lymph node levels was 85% and 62%, respectively (Table 4).

False-positive findings were obtained with immuno-PET (two levels), CT (two levels), and MRI (one level). No false-positive cases were observed with palpation and FDG-PET.

The paraffin slides of the seven tumor-involved lymph node levels that had been missed with immuno-PET were reexamined by histopathologic examination (Table 5). The tumor-involved lymph nodes found in these levels were relatively small and contained just a small proportion of tumor tissue. No necrosis was observed in these tumors. Six of seven tumor-involved lymph node levels that had been missed by immuno-PET were also missed by CT and/or MRI. The smallest tumor-involved lymph node detected by immuno-PET was 5×5 mm, with 75% tumor involvement.

Discussion

Immuno-PET combines the high resolution of PET with the high specificity and selectivity of mAbs. This makes immuno-PET an attractive modality for tumor detection. In addition, immuno-PET can also be used in a therapeutic setting with mAbs for confirmation of tumor targeting and for quantitative dose calculations. The possibility for combined use of mAbs in tumor detection, therapy planning, and therapy makes the position of immuno-PET fundamentally different from FDG-PET.

In the current study, the long-lived positron emitter ^{89}Zr was evaluated for the first time ever in a clinical immuno-PET trial. ^{89}Zr was coupled to cmAb U36 via the bifunctional chelate *N*-succinyldesferrioxamine B. Modification procedures were

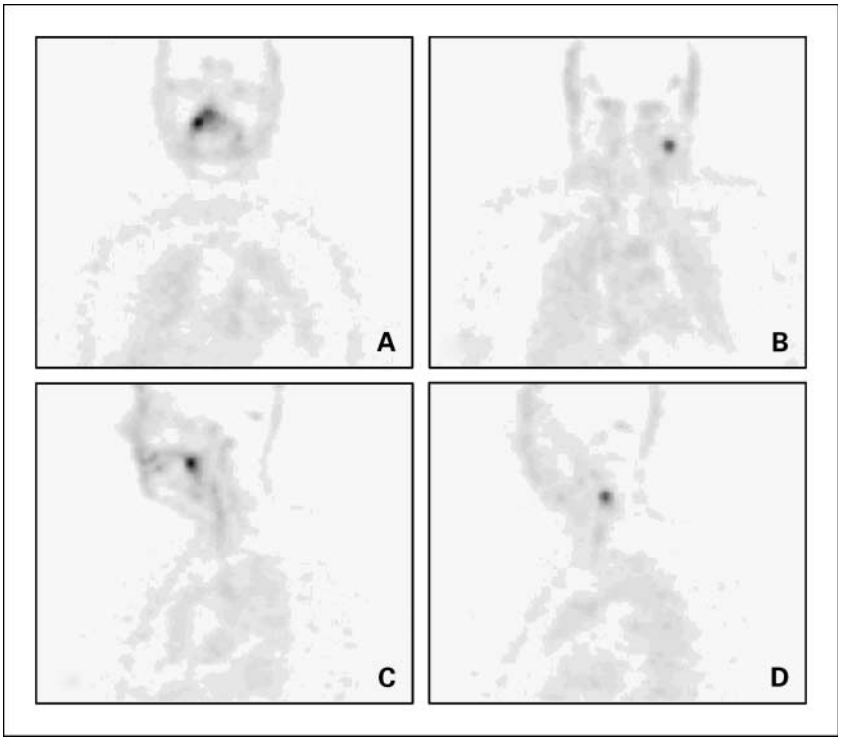

Fig. 3. Immuno-PET images with ^{89}Zr-cmAb U36 of head and neck cancer patient 19, with a tumor on the right side of the soft palate, and a lymph node metastasis at the left side of the neck (level III). Images were obtained 72 hours postinjection. *A,* coronal image of primary tumor; *B,* coronal image of lymph node metastasis in the neck; *C,* sagittal image of primary tumor; *D,* sagittal image of lymph node metastasis in the neck.

Table 2. Correlation of preoperative findings with histopathologic findings per level

121 operated levels, 25 tumors involved	Sensitivity	Specificity	Accuracy
Palpation	11/25 (44%)	96/96 (100%)	107/121 (88%)
CT/MRI	15/25 (60%)	94/96 (98%)	109/121 (90%)
^{89}Zr-immuno-PET	18/25 (72%)	94/96 (98%)	112/121 (93%)

standardized to arrive at a chelate/mAb molar ratio <2. No impairment of the immunoreactivity of cmAb U36 was observed upon radiolabeling. Administration of ^{89}Zr-cmAb U36 (75 MBq, 10 mg) to HNSCC patients seemed to be safe. Just 2 of 20 patients showed an antibody response directed against cmAb U36, while in a previous radioimmunotherapy study this was 5 of 12 after administration of 50 mg radiolabeled cmAb U36. No evidence was found for antibody reactions against the chelate.

Immuno-PET with ^{89}Zr-cmAb U36 seemed to be a promising method for imaging of primary head and neck tumors as well as metastases in the neck. All primary tumors were visualized, whereas 18 of 25 tumor-containing neck levels were also identified. In this feasibility study, the sensitivity of immuno-PET for detection of lymph node metastases was at least as good as of CT/MRI: 72% versus 60%. In a previous SPECT study with ^{99m}Tc-labeled mmAb U36 in a comparable group of patients, a sensitivity of 50% was found for nuclear imaging, the same as for CT and MRI. Because the number of patients in both studies was small, it is not justified to compare the performance of ^{89}Zr-immuno-PET and ^{99m}Tc-SPECT just on the basis of sensitivity percentages. Nevertheless, it became clear from the present study that ^{89}Zr-immuno-PET performs better with respect to tumor delineation. One reason for this is the better spatial resolution of PET. ^{89}Zr-immuno-PET showed detailed delineation of organs like heart as well as of tumors and blood vessels (Fig. 1). This had not been the case with ^{99m}Tc-SPECT (3). Another reason for better delineation is the longer half-life of ^{89}Zr than of ^{99m}Tc (78.4 versus 6.0 hours), which allowed imaging at later time points, when tumor-to-nontumor radioactivity uptake ratios are higher (Fig. 1). Indeed, in the present study, delineation of primary tumors and lymph node metastases was better at later time points (72 and 144 hours) than at earlier time points (data not shown). Image quality might be further improved by elongation of the scanning time for the two bed positions covering the head and neck region.

Table 3. Correlation of preoperative findings with histopathologic findings per side

25 operated sides, 15 tumors involved	Sensitivity	Specificity	Accuracy
Palpation	8/15 (53%)	10/10 (100%)	18/25 (72%)
CT/MRI	11/15 (73%)	9/10 (90%)	20/25 (80%)
^{89}Zr-immuno-PET	11/15 (73%)	8/10 (80%)	19/25 (76%)

Table 4. Correlation of preoperative findings with histopathologic findings per level in six patients who received FDG-PET

40 operated levels, 13 tumors involved	Sensitivity	Specificity	Accuracy
Palpation	7/13 (54%)	27/27 (100%)	34/40 (85%)
CT/MRI	10/13 (77%)	27/27 (100%)	37/40 (93%)
FDG-PET	8/13 (62%)	27/27 (100%)	35/40 (88%)
^{89}Zr-immuno-PET	11/13 (85%)	27/27 (100%)	38/40 (95%)

Although good resolution is an advantage, it is fair to say that immuno-PET is hampered by the lack of anatomic structures. For example, because of the slow clearance of the conjugate from the blood, it might be difficult to distinguish a targeted lymph node metastasis from a cross-section through a blood vessel. In the present study, no explanation was found for the two false-positive observation with ^{89}Zr-immuno-PET. An improvement in image interpretation might be obtained by fusion of immuno-PET images with CT or MRI images. This approach enables the combination of (tumor) biological and anatomic information. We explored this approach for a few patients, including patient 16 with extensive bilateral lymph node involvement (Fig. 2). Figure 4 shows the fused PET-CT image of the same patient 16, and the fusion makes clear that increased uptake of ^{89}Zr-cmAb U36 indeed is confined to the enlarged lymph nodes in the neck. To get a proper match between the immuno-PET and CT images, the head of this patient had to be fixed in the same way during both imaging procedures by using a thermoplastic radiotherapy mask. Problems related to matching will be solved when PET imaging and anatomic CT or MRI imaging are done simultaneously by use of hybrid scanners. The use of combined PET/CT scanners is rapidly expanding and first efforts in developing MRI-compatible PET scanners have been reported (16). The availability of anatomic data will not only provide landmarks for PET image interpretation, but can also be used for more accurate quantification of mAb distribution (e.g., partial volume correction).

Table 5. Tumor involvement of tumor containing levels missed by immuno-PET

Patient no., level	Size (mm)	%Tumor	Remarks
1, level II	7 × 11	25	Missed by MRI/detected by CT
3, level III	9 × 15	50-75	Missed by CT/MRI
5, level III	4 × 4	10	Missed by CT/MRI
	8 × 15	10	
6, level II	5 × 7	5	Missed by CT/MRI
	6 × 8	50-75	
	5 × 9	5	
7, level I	5 × 7	5	Missed by CT (no MRI)
14, level IV	8 × 12	10-25	Missed by CT/MRI
15, level II	5 × 5	25-50	Detected by CT/MRI

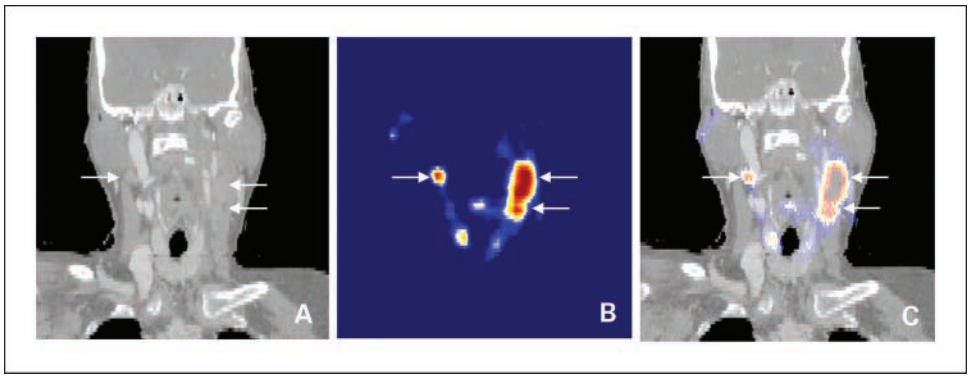

Fig. 4. Fusion (*C*) of CT (*A*) and coronal immuno-PET (*B*) images of head and neck cancer patient 16 (same as in Fig. 2), with a tumor in the left tonsil and lymph node metastases at the left (level II and III) and right (level II) side of the neck. Images were obtained 72 hours postinjection. In these slices, only lymph node metastases are visible.

Following this feasibility study, the exact position of immuno-PET using ^{89}Zr-cmAb U36 within the current armamentarium for diagnosis of head and neck cancer still has to be established. One has to realize that apart from noninvasive imaging methods for the neck, invasive diagnostic procedures are also available, e.g., ultrasound-guided fine-needle aspiration cytology. In ultrasound-guided fine-needle aspiration cytology, selection of lymph nodes to be aspired is based on known patterns of lymphatic spread and/or lymph node size and morphology as assessed with ultrasound, sometimes after obtaining evidence by CT or MRI scan. Although ultrasound-guided fine-needle aspiration cytology enables detection of lymph node metastases at a single-cell level, it has also some unfavorable aspects, however: (*a*) Its accuracy is strongly dependent on the skills of the ultrasonographer and the cytopathologist, (*b*) it is an invasive method, and (*c*) it gives only information of a selected part of the neck and not on the primary tumor or distant metastases.

At the current stage of development, immuno-PET with ^{89}Zr-cmAb U36 is not able to detect micrometastases in the neck, an observation that has also been previously reported for FDG-PET (17, 18). False-negative observations in the present study were mostly due to the presence of small metastatic lymph nodes with minimal tumor involvement (Table 5), whether or not such small tumors are efficiently targeted by mAb U36, as previously shown in a biodistribution study with mmAb U36 (19).

From a diagnostic point of view, immuno-PET with ^{89}Zr-cmAb U36 might also have perspectives for the detection of distant metastases. Approximately 25% of advanced-stage (stage III and IV) head and neck cancer patients develop distant metastases. Because surgical management is reserved for patients with locoregional disease, the presence of distant metastases is critical and may significantly influence treatment. Recent studies have shown that there is a role for FDG-PET in the detection of occult distant metastases (20). It can be anticipated, however, that the use of immuno-PET with ^{89}Zr-labeled mAbs might add another dimension to the detection of distant metastases, especially when the same mAb is used for systemic therapy. Within such a strategy, immuno-PET might play a dual role: tumor detection as well as treatment planning.

mAbs are gaining momentum for the use in tumor-selective systemic therapy, also for treatment of head and neck cancer. Presently, 17 mAbs (all intact IgGs) have been approved by the Food and Drug Administration for therapy, most of them for systemic treatment of cancer. Of the approved mAbs, cetuximab (directed against the epidermal growth factor receptor) and bevacizumab (directed against the vascular endothelial growth factor) are also used in strategies for treatment of head and neck cancer. In addition, several other mAbs are under evaluation for therapy of head and neck cancer, such as the radiolabeled mAbs U36 (4, 5) and L19. The latter mAb is directed against the ED-B domain of fibronectin, and capable of selective targeting of tumor neovasculature (21–23). Data presented in this initial clinical feasibility study justify further exploration of ^{89}Zr-immuno-PET as an imaging tool for the selection of high-potential candidate mAbs for therapy as well as of patients most likely to benefit from (expensive) mAb treatment.

Acknowledgments

We thank the staff of BV Cyclotron (VU University) for supply of ^{89}Zr, Dr. Jan H. Rector (Solid State Physics, VU University) for sputtering ^{89}Y on copper supports, Drs. Gerard W.M. Visser and Iris Verel for advice on radiochemistry, Ing. Henri N.J.M. Greuter for pharmacokinetic determinations, Dr. Bram J. Wilhelm for pharmacokinetic modeling, Ing. Marijke Stigter for human antichimeric antibody analyses, Dr. Jan C. de Munck for image fusion, Dr. D. Joop Kuik for advise on statistics, and Dr. Manfred van der Vlies for supervision of radiation safety issues.

References

1. Zuckier LS, DeNardo GL. Trials and tribulations: oncological antibody imaging comes to the fore. Semin Nucl Med 1997;27:10–29.
2. Goldenberg DM. Advancing role of radiolabeled antibodies in the therapy of cancer. Cancer Immunol Immunother 2003;52:281–96.
3. De Bree R, Roos JC, Quak JJ, Den Hollander W, Snow GB, Van Dongen GAMS. Radioimmunoscintigraphy and biodistribution of ^{99m}Tc-labeled monoclonal antibody U36 in patients with head and neck cancer. Clin Cancer Res 1995;1:591–8.
4. Colnot DR, Quak JJ, Roos JC, et al. Phase I therapy study of ^{186}Re-labeled chimeric monoclonal antibody U36 in patients with squamous cell carcinoma of the head and neck. J Nucl Med 2000;41:1999–2010.
5. Colnot DR, Ossenkoppele GJ, Roos JC, et al. Reinfusion of unprocessed, granulocyte colony-stimulating factor-stimulated whole blood allows dose escalation of ^{186}Re-labeled chimeric monoclonal antibody U36 radioimmunotherapy in a phase I dose escalation study. Clin Cancer Res 2002;8:3401–6.
6. Eary JF. PET imaging for planning cancer therapy. J Nucl Med 2002;42:764–9.
7. Lee FT, Scott AM. Immuno-PET for tumor targeting. J Nucl Med 2003;44:1271–81.
8. Verel I, Visser GWM, Van Dongen GAMS. The promise of immuno-PET in radioimmunotherapy. J Nucl Med 2005;46:164–71S.
9. Verel I, Visser GWM, Boellaard R, Stigter-van Walsum M, Snow GB, Van Dongen GAMS. ^{89}Zr immuno-PET: comprehensive procedures for the production of ^{89}Zr-labeled monoclonal antibodies. J Nucl Med 2003;44:1271–81.
10. Verel I, Visser GWM, Boellaard R, et al. Quantitative ^{89}Zr-immuno-PET for *in vivo* scouting of ^{90}Y-labeled monoclonal antibodies. J Nucl Med 2003;44:1663–70.
11. De Bree R, Roos JC, Quak JJ, Den Hollander W, Snow GB, Van Dongen GAMS. Clinical screening of monoclonal antibodies 323/A3 (K931), cSF-25

(K984), and K928 for suitability of targeting tumors in the upper-aerodigestive and respiratory tract. Nucl Med Commun 1994;15:613–27.

12. Sobin LH, Wittekind Ch, editors. TNM classification of malignant tumors 6th edition. International Union Against Cancer. New York: Wiley-Liss; 2002.

13. Heider KH, Mulder JW, Ostermann E, et al. Splice variants of the cell surface glycoprotein CD44 associated with metastatic tumour cells are expressed in normal tissues of humans and cynomolgus monkeys. Eur J Cancer 1995;31A:2385–91.

14. Van den Brekel MWM, Stel HV, Castelijns JA, et al. Cervical lymph node metastases: assessment of radiological criteria. Radiology 1990;177:379–84.

15. Robbins KT, Clayman G, Levine PA, et al. American Head and Neck Society; American Academy of Otolaryngology and Head and Neck Surgery. Neck dissection classification update: revisions proposed by the American Head and Neck Society and the American Academy of Otolaryngology and Head and Neck Surgery. Arch Otolaryngol Head Neck Surg 2002;128:751–8.

16. Marsden PK, Strul D, Keevil SF, Williams SCR, Cash D. Simultaneous PET and NMR. Br J Radiol 2002;75:S53–9.

17. Stoeckli SJ, Steinert H, Pfaltz M, Schmid S. Is there a role for positron emission tomography with ^{18}F-fluorodeoxyglucose in the initial staging of nodal negative oral and oropharyngeal squamous cell carcinoma. Head Neck 2002;24:345–9.

18. Brouwer J, De Bree R, Comans EFI, et al. Positron emission tomography using [^{18}F]fluorodeoxyglucose (FDG-PET) in the clinically negative neck: is it likely to be superior. Eur Arch Otorhinolaryngol 2004;261:479–83.

19. De Bree R, Roos JC, Quak JJ, et al. Selection of monoclonal antibody E48 IgG or U36 for adjuvant therapy in head and neck cancer patients. Br J Cancer 1997;75:1049–60.

20. Regelink G, Brouwer J, De Bree R, et al. Detection of unknown primary tumors and distant metastases in patients with cervical metastases: value of FDG-PET versus conventional modalities. Eur J Nucl Med Mol Imaging 2002;29:1024–30.

21. Birchler MT, Milisavlijevic D, Pfaltz M, et al. Expression of the extra domain B of fibronectin, a marker of angiogenesis, in head and neck tumors. Laryngoscope 2003;113:1231–7.

22. Neri D, Bicknell R. Tumour vascular targeting. Nat Rev Cancer 2005;5:436–46.

23. Santimaria M, Moscatelli G, Viale GL, et al. Immunoscintigraphic detection of the ED-B domain of fibronectin, a marker of angiogenesis, in patients with cancer. Clin Cancer Res 2003;9:571–9.